Charting the irreversible degradation modes of low band gap Pb-Sn perovskite compositions for de-risking practical industrial development

Christina Kamaraki[1,2], Matthew T. Klug[1], Vincent J.-Y. Lim[3], Nourdine Zibouche[5], Laura M. Herz[3,4], Saiful Islam[6], Christopher Case[1,*] and Laura Miranda Perez[1,*]

[1]Oxford Photovoltaics Ltd, Unit 7/8 Mead Road, Yarnton, OX5 1QU, United Kingdom

[2]Department of Physics, University of Bath, Claverton Down, Bath BA2 7AY, United Kingdom

[3]Department of Physics, University of Oxford, Clarendon Laboratory, Parks Road, Oxford OX1 3PU, United Kingdom

[4] Institute for Advanced Study, Technical University of Munich, D-85748 Garching, Germany

[5]Department of Chemistry, Lancaster University, Bailrigg, LA1 4YB, United Kingdom

[6]Department of Materials, University of Oxford, Parks Road, Oxford, OX1 3PH, United Kingdom

*Authors to whom correspondence should be addressed: laura.miranda@oxfordpv.com, chris.case@oxfordpv.com

Abstract

The commercialization of a solar technology necessitates the fulfilment of specific requirements both in terms of efficiency and stability in order to enter and gain space in the photovoltaic (PV) market. These aims are heavily dependent on the selection of suitable materials, which is critical for suppressing any reliability risks arising from inherent instabilities. Focusing on the absorber material, the main core of a PV device, herein we investigate which is the most suitable low bandgap lead-tin composition candidate for all-perovskite tandem applications by studying their degradation mechanisms with both widely available and advanced characterization techniques. We identify three irreversible degradation processes in narrow band gap Pb-Sn perovskite absorbers: (1) Sn oxidation upon air exposure, (2) methylammonium (MA) loss upon heat exposure, and (3) formamidinium (FA) and cesium (Cs) segregation leading to impurity phase formation. From an industrial perspective, we therefore propose to refocus attention on $FASn_{0.5}Pb_{0.5}I_3$ which minimizes all three effects while maintaining a suitably low bandgap for a bottom cell and good photovoltaic performance. Moreover, we propose a practical and highly sensitive characterization method to monitor the oxidation evolution, which can be deployed both in laboratory and industrial environments and provide useful information for the technological development process, including the quality of the absorber, the effectiveness of encapsulation methods, and the acceptable time windows for air exposure.

Introduction

One of the most promising routes to overcome the practical efficiency limits of mainstream solar technology is the multi-junction concept that employs multiple solar absorbers to minimize thermalization losses and use sunlight more efficiently. The high photovoltaic (PV) performance and low-cost processing of metal halide perovskite absorbers make them a promising technology for the cost-competitive introduction of tandem (*i.e.*, two-junction) modules into the terrestrial solar market. The outstanding certified efficiencies of 28.6% and 33.7% for perovskite-on-silicon tandems on a full M4 wafer (258.15 cm^2) and lab-scale (1 cm^2) device, respectively, together with the near-future expectation of market entry for Si-based tandems in industry projections such as the International Technological Roadmap for Photovoltaics (ITRPV) showcase both the potential and maturity level of tandem technology.[1],[2],[3,4] While perovskite-on-silicon tandems will lead the entry of perovskite technology into the solar market, the narrowing of the perovskite band gap through partial Pb-site

substitution by Sn in the $APbX_3$ perovskite lattice enables all-perovskite tandems, whereby silicon is replaced, as the bottom-cell absorber material. The current record efficiency of 28% for an all-perovskite tandem nearly matches the record performance of silicon and demonstrates that this technology has the potential to out-perform it.[5,6] The all-perovskite tandem concept offers independence from the silicon supply chain, the use of deposition routes beyond those employed in wafer-based processing, as well as the opportunity to make flexible thin-film modules for lightweight applications. Multiple Pb-Sn perovskite compositions can achieve the required band gap for a bottom-cell and have demonstrated high performances exceeding 20%. However, the community has yet to align on a preferred choice of material stoichiometries.[7–12]

The material stability and PV efficiency of perovskite solar absorbers are highly dependent on composition. While formamidinium lead iodide,$FAPbI_3$, achieves record-setting performance in single-junction devices, in absence of special techniques to stabilize the required crystallographic alpha-phase it would readily transition into the non-perovskite delta-phase and lose functionality.[13–19] In contrast, the 1.7-1.8 eV band gap compositions used for the top-cell absorber in high performance perovskite-based tandem cells are achieved by using a mixture of cations at the A-site in combination with a mixture of halides at the X-site. While the role of the A-site cation is often described as that of a spacer ion with an effective ionic radius that satisfies the tolerance criteria for forming the perovskite crystal structure, this is an oversimplification. In addition to stabilizing the desired crystallographic phase[18,20–22], certain choices of the A-site cation can also suppress ion migration[21,23–26] , minimize halide segregation[27–29], induce octahedral distortions[30–32], and improve structural cohesion [33,34] as well as charge transport properties.[35–37] The shape, size, and chemical nature of the A-site ions can induce local and global lattice deformations that either promote or suppress the formation of defects. This choice not only impacts optoelectronic quality but could also open or close pathways for the movement of ions intrinsic to the perovskite absorber and extrinsic molecules such as oxygen and water through the absorber. [22,38,39] To date, prior work has studied the role of the A-site cation almost exclusively in neat Pb perovskite absorbers, whereas it is largely unclear whether it would influence the more complex mixed-metal Pb-Sn perovskites to a greater or lesser degree. Narrowing the band gap of metal halide perovskites below about 1.55 eV requires the partial substitution of Pb(II) at the B-site by Sn(II), which is inherently susceptible to oxidation and vacancy formation, thereby introducing new, yet primary, degradation modes not present in neat Pb perovskite compositions. While many strategies have emerged to mitigate the practical effects of Sn(II) oxidation, such as the introduction of reducing agents[40–43], tin compensators like SnF_2[44–47], or comproportionation[48], there has been little attention focused on how the A-site choice might influence inherent material degradation modes. Over the course of their manufacture and operation, solar cells will experience at various points the extrinsic stressors of heat, light, and atmosphere. While proper encapsulation can minimize atmospheric exposure during operation, it is extremely costly to prevent any oxygen or moisture exposure from occurring during high-throughput manufacturing. Therefore, it is critical that the practical failure modes that could arise from A-site cation selection be identified so that a “de-risked” perovskite composition is selected as the baseline for launching industrial research and development efforts. Looking towards production, not only will the low-band-gap perovskite absorbers need to maintain competitive power output and operational lifetimes with proven technologies, but practical and affordable characterization methods are required to monitor the progression of degradation for industrial quality control.

Herein, we explore a set of nine compositions around the band gap minimum of the $A(Sn_xPb_{1-x})I_3$ series to assess how common A-site compositions and B-site compositions impact material degradation under heat and air exposure. By characterizing samples before and after stressing with widely and industrially available techniques, such as X-ray diffraction (XRD) and spectrophotometry, we observed

that A-site cation choice can impact material stability. Moreover, we further investigate the nature of these degradation routes by employing advanced techniques such as density functional theory (DFT) calculations and terahertz (THz) photoconductivity spectroscopy to gain insights about how the A-site ions interact with oxygen at the atomic scale and impact key optoelectronic properties that govern photovoltaic operation, respectively. With the view towards manufacturing, we also highlight how lateral conductivity offers a signal that is highly sensitive to oxygen exposure and could be easily integrated into encapsulated devices, thereby providing a useful means for quality control and assessing the effectiveness of encapsulation methods used for commercial products.

Results

A set of nine narrow-band-gap Pb-Sn perovskite compositions were investigated across the full matrix of three A-site compositions ($FA_{0.75}Cs_{0.25}$, $FA_{0.6}MA_{0.4}$, and FA) and three B-site compositions ($Sn_{0.5}Pb_{0.5}$, $Sn_{0.6}Pb_{0.4}$, and $Sn_{0.7}Pb_{0.3}$). Thin films of each of the compositions studied were prepared in an inert atmosphere by spin-coating with an anti-solvent quench (see the Methods Section for details). Powder XRD was performed on the set of thin films and the measured patterns, shown in Figure 1a, indicate that all compositions adopt the same pseudocubic crystal structure, and no additional phases or crystalline impurities are observed. Figure 1b shows how the Sn content and A-cation choice impact the peak position of the perovskite (100) reflection. Regardless of A-cation choice, the perovskite XRD peak shifts to higher diffraction angles as the Sn content increases, which indicates lattice contraction, consistent with the incorporation of the smaller sized Sn^{2+} ion at the B-site and aligns with previous reports[32,49]. Similarly, the peak position shifts to lower angles, indicating lattice expansion, as the effective ionic radius of the A-cation increases from FA/Cs to FA/MA, then to FA. Under the processing conditions used, the FA/MA compositions demonstrate stronger preferred orientation of the (100) planes, as evidenced by a higher (100)/(111) peak intensity ratio compared to that for their FA/Cs counterparts (Figure S6). Figure 1c confirms that the band gap of all different compositions, as determined by the first derivative peak of each composition's absorption spectrum, is around 1.3 eV and thereby suitable as low band gap absorbers in perovskite multi-junction solar cells[50]. While the values are similar, the finer variations in band gap will depend on the interplay between octahedral tilting and lattice contraction/expansion that is induced by the introduction of a smaller/larger cation at the A-site and B-site.[32] Scanning electron microscopy confirmed that pinhole-free films were obtained for all compositions (Figure S7).

Over the course of solar cell manufacture and operation in the field, the perovskite absorber will experience heat and air exposure to different degrees. To make a practical assessment of how heat and air exposure impacts the bulk material properties of each perovskite composition, thin film samples were stressed either by heating at 100°C under inert atmosphere or by exposure to ambient air at room temperature and 40% relative humidity. The time evolution of their crystal structure and absorption spectra were periodically measured by powder XRD and UV-visible-NIR spectrophotometry. Figure 2a displays the time-evolution of XRD patterns for FA/MA, FA and FA/Cs-based compositions with 50% Sn content during thermal stressing. Of the compositions considered, the FA/MA A-cation choice is the least thermally stable since an impurity peak at 2θ = 12.6° corresponding to PbI_2 emerges and grows in intensity as the main perovskite peak at ~14° reduces. In contrast, the XRD patterns of the FA and FA/Cs compositions remain unchanged after 72 hours. We find that this same behaviour occurs for the compositions with 60% and 70% Sn content, which reveals that the thermal stability is primarily dependent on the A-site cation composition (Figure S8) and is consistent with MAI sublimation from the perovskite absorber.[51–55] This finding is also supported by spectrophotometry measurements of the absorption spectra. Figure 2c displays the derivative of

the absorption spectra and shows that the peak position and breadth of FA and FA/Cs are invariant during thermal stressing, whereas the derivative for FA/MA compositions shifts to longer wavelengths and broadens over time, which respectively indicate a band gap narrowing, consistent with FA-enrichment as MAI leaves and an increase in band edge disorder over the course of thermal stressing. Likewise, the absorption spectra for FA/MA compositions also show a reduction in absorption (Figure S9) above the band gap, which is consistent with the XRD observations of perovskite material loss and PbI_2 formation (Figure 2a and S8).

Figure 2d shows the time evolution of the XRD pattern upon ambient air exposure for each composition around the (100) perovskite peak. A gradual reduction in peak intensity over 72 hours of exposure is observed in all cases regardless of the A-cation choice. The rate of XRD intensity decrease is correlated with Sn percentage as higher Sn content compositions exhibiting faster peak intensity reductions (Figure S10 and S12). Additionally, significant widening of the 14^o peak with increasing Sn content is observed upon air exposure, but only minor variations are observed upon heat stressing (Figure S14). These trends in peak intensity breadth are consistent with the degradation process of the perovskite absorber due to the oxidation of Sn^{2+} at the B-site, with the broadening indicating the crystallographic disorder increases alongside these local compositional changes.[56,57] Interestingly, for any given Sn concentration, the broadening is substantially reduced for the FA-only system compared to the mixed A-site compositions. This suggests that the process of oxidation induces higher degree of local lattice rearrangement in the FA/MA and FA/Cs mixed systems than in the FA only compositions. Although no crystalline degradation products related to Sn^{4+} species were detected, amorphous SnO_2 may have formed as it has been reported in previous studies, thus leaving behind Sn-vacancies that preserve the overall perovskite structure. [56,58,59] While all compositions show a perovskite peak intensity decrease with atmospheric stressing, only the FA/Cs compositions show a significant monotonic shift to lower diffraction angles. In particular, the final peak position after 72 hours of stressing almost coincides with that for the FA-based composition. Additionally, the δ-$CsPbI_3$ phase has emerged in the powder XRD pattern at $2\vartheta = 26^o$ (Figure 2d – inset), which indicates that Cs segregates from the lattice to form the δ-$CsPbI_3$ impurity phase, thereby leaving behind an FA-enriched perovskite with an expanded lattice. In contrast to the XRD measurements, which clearly show that the perovskite crystal structure is largely preserved even after prolonged air exposure, the absorption spectra show that the optoelectronic properties are severely degraded. Figure 2e and f present the absorption spectra for the $FA_{0.75}Cs_{0.25}Sn_{0.5}Pb_{0.5}I_3$, $FA_{0.6}MA_{0.4}Sn_{0.5}Pb_{0.5}I_3$, and $FASn_{0.5}Pb_{0.5}I_3$ compositions and their corresponding first derivative peaks in the near-IR region around the band edge. Whereas a clear absorption edge can be defined by a prominent peak in the first derivative for pristine samples, within 24h of humid air exposure the edge has substantially broadened to the point that a first derivative peak is hardly distinguishable and has blue-shifted by approximately 10 nm. This apparent band gap widening is consistent with Pb-enrichment and electronic defect generation as Sn^{2+} oxidizes to Sn^{4+} and becomes excluded from the perovskite lattice. After 24h, the first derivative peak has disappeared, thereby indicating that the perovskite band gap has become a continuum of defect states. This trend is the same regardless of the composition (Figure S11). Thus, it is evident that what appears to be a minimal absorber degradation in the XRD actually corresponds to a severely impaired optoelectronic quality. Similar trends were also reported for in-operando XRD measurements performed in parallel with electrical characterization of devices under stressing, where significant changes in the current-voltage characteristics were observed while the XRD pattern remained the same.[60]

While the XRD and spectrophotometry data make it phenomenologically clear that exposure to ambient air poses the primary degradation mode for all of the Pb-Sn compositions considered, it is also evident that Cs can influence the degradation pathway of the perovskite material. In order to

shed more light on the possible interactions that can occur between oxygen and A-site cations on the atomic-scale, ab-initio computational methods based on of Density Functional Theory (DFT) were employed. The atomistic influence of oxygen and iodide vacancies has not been fully addressed for Pb-Sn perovskites. By positing that the degradation process involving superoxide species as in $MAPbI_3$[61] might also proceed for Pb-Sn perovskites, we used DFT to compare how $FASn_{0.5}Pb_{0.5}I_3$ and $FA_{0.75}Cs_{0.25}Sn_{0.5}Pb_{0.5}I_3$ would respond when an iodide vacancy is occupied by an O_2^- superoxide species (computational details are provided in the Methods section).

Initially, we found that $FASn_{0.5}Pb_{0.5}I_3$ is marginally more stable than $FA_{0.75}Cs_{0.25}Sn_{0.5}Pb_{0.5}I_3$ with a relative energy difference of about 70meV. Upon oxygen incorporation, we considered three different O_2^- substitution sites of the iodine vacancy in the $FASn_{0.5}Pb_{0.5}I_3$ structure; these are between Sn atoms (Sn-O_2-Sn), between Pb atoms (Pb-O_2-Pb), and between Sn and Pb atoms (Sn-O_2-Pb) as shown in Figure S15. In the case of $FA_{0.75}Cs_{0.25}Sn_{0.5}Pb_{0.5}I_3$, we also examined the proximity effect of the O_2^- species with the Cs atom (Figure S16). By analysing the local structures and relative energies of the different O_2^- substitution sites, we found that the superoxide, O_2^-, species has an energetic preference (by 60 to 200meV) to coordinate to Sn atoms (Table S2). Interestingly, for the $FA_{0.75}Cs_{0.25}Sn_{0.5}Pb_{0.5}I_3$ system the energetics also indicate that the O_2^- species prefers to be located away from the Cs atoms. The preference of the superoxide to sit near Sn^{2+} and FA^+ cations provides a possible explanation for why the δ-$CsPbI_3$ phase is observed in the XRD patterns for FA/Cs compositions upon air exposure. We hypothesize that by eschewing the Cs ions, even in a chemically homogeneous perovskite lattice, oxidation would target defects near Sn and FA cations and initiate a segregation process that destabilizes A-site and B-site mixing and promote Cs and Pb enrichment elsewhere, eventually leading to the emergence of the crystalline δ-$CsPbI_3$ phase.

While monitoring how air exposure influences the absorption edge through spectrophotometry has highlighted that the optoelectronic quality of all Pb-Sn perovskite compositions degrades much more quickly than its crystal structure, it is not the most directly relevant metric of semiconductor properties for photovoltaic systems. Thus, terahertz spectroscopy optical-pump terahertz-probe (OPTP) measurements were performed to monitor carrier-charge transport properties as a function of ambient air exposure over time. In OPTP, a thin film perovskite sample is photoexcited with an ultrafast pump laser pulse before its time-dependent photoconductivity is measured with a THz conductivity probe, as is detailed in the Methods section. Utilising the photoconductivity traces (full dataset provided in Figure S1-S4 in the SI), the sum charge-carrier mobility can be extracted from the THz pulse transmission immediately after photoexcitation. The charge-carrier recombination rates, k_1, can also be extracted from monoexponential fits to photoconductivity decays, which is representative of the charge-carrier population. Figure 3 shows the monoexponential decay rate and sum charge-carrier mobility from such analysis (Figure S1-S4) for both the FA/Cs and FA/MA compositions at varying air-exposure times. Although all the Pb-Sn perovskites show high initial mobility values around 30 cm^2/Vs, consistent with literature[62,63], after 5 hours of exposure the values decrease to 20 cm^2/Vs. Given that the OPTP technique is only sensitive to scattering in the order of nanometres, we interpret this to mean that the thin films still retain a relatively high degree of short-range crystalline order after prolonged air exposure. In contrast, the increase of k_1 by 1-2 orders of magnitude during air exposure reveals that the charge-carrier recombination increases exponentially with exposure time, and this indicates that the perovskite materials are becoming increasingly defective. For these intermediate Pb-Sn compositions, such accelerated decay is likely to be associated with defect formation, resulting in either charge-carrier trapping, or the formation of tin vacancies that capture valence-band electrons thus leading to hole doping[64]. The effect of these findings on the charge-carrier transport is made obvious in Figure 3 by plots of charge-carrier diffusion length, L_D, which can

be estimated by $L_D = \sqrt{\mu k_b T / q\, k_1}$. We find that FA/Cs compositions initially exhibit higher charge-carrier diffusion lengths than FA/MA, but after about 1 hour of air exposure the compositions converge to a shared decay profile. These measurements provide a finer time resolution with which to observe the oxidation process that reduces the optoelectronic quality than our previous assessments and reveal that the characteristic time scale of degradation relevant to charge-carrier transport is about 30 minutes.

We further performed terahertz time-domain spectroscopy (THz-TDS) at different air exposure times (see SI for details), in order to measure the conductivity spectra of the perovskite films in absence of any photoexcitation. Such measurements of the dark conductivity spectra can provide information about the background charge-carrier density, as well as vibrational phonon modes present within the THz spectral region. We find that the dark conductivity spectra of the perovskite compositions under consideration do not exhibit any significant changes with air exposure times, suggesting that electrical doping induced from degradation does not exceed 10^{18}cm^{-3}, which is the lower limit imposed by the sensitivity of the THz-TDS measurements (Figure 3 and Figure S5). However, it is expected from other reports that the oxidation of Sn^{2+} at the B-site leads to p-doping and the generation of a background hole population to charge compensate the Sn-vacancies.[58,62,65–67] Therefore, an alternative method for monitoring and quantifying the evolution of the background charge-carrier concentration below the THz-TDS detection limit is required for tracking the oxidation process in real-time.

A relatively simple and inexpensive method with high enough sensitivity and dynamic range to capture large changes in charge transport over the course of hours is lateral conductivity.[12,68] Perovskite films were deposited onto substrates that have been patterned with interdigitated electrodes of several different channel lengths between 50 and 150 µm and the resistivity through the perovskite film across the channel widths was determined electronically. Figure 4a demonstrates the conductivity profiles versus time for FA perovskites of different Sn content, revealing similar behaviour for each composition. Initially, an increase in σ values is observed by 2-3 orders of magnitude to reach a maximum value, σ_{max}, around 10^{-1} S/cm, which then decreases by several orders of magnitude until stabilizing around 10^{-8} S/cm, which is near the threshold for detection. We attribute the initial conductivity rise to p-doping of the material arising from Sn-vacancy formation and the capture of electrons at the corresponding sites, leading to hole doping in the valance band.[44,59,64] Similar trends are observed also for the mixed A-cation compositions FA/MA and FA/Cs as displayed in Figure S17. In Figure 4b, we characterize the conductivity rise by reporting the initial and maximum conductivity values, σ_i and σ_{max}, as well as the time to reach σ_{max}, T_{max}, for each of the compositions and find that it is primarily dependent on Sn concentration. Using the mobility values measured by OPTP, we estimate a background hole density of approximately 10^{16} cm^{-3} corresponding to the peak conductivity values shown in Figure 5, which is indeed below the THz-TDS detection limit. We interpret the sharp decline in conductivity values observed in Figure 4a as the disruption of lateral charge percolation pathways along the perovskite layer as the material degrades upon prolonged air exposure. We observe in Figure 4a that the initial conductivity increases and the time to reach the maximum value along with the subsequent decay time shortens with increasing Sn content regardless of A-cation choice. By separately fitting the initial rise and final decay of the peak with monoexponential functions, we observe that the respective characteristic rise and decay times, τ_1 and τ_2, are longer for 50% Sn compared to those with the 60% Sn counterpart (Figure S18). Moreover, the intersection point of the fitting curves almost coincides with the time needed to reach σ_{max} in both cases, indicating that the peak can be interpreted as the competition of two mechanisms: doping is initially dominant, but when oxidation has proceeded long enough, the generated SnO_2 disrupts the charge percolation pathways and impedes lateral charge carrier collection. Further modeling could

give more insights on the fundamental understanding of this behavior; however, it is beyond the scope of this work.

Despite being fabricated in a nominally oxygen- and humidity-free environment, the greater the Sn content, the more likely the film is to be either initially oxidized upon formation by residual oxygen or to oxidize during the few minutes it takes to load the sample for measurement in air. Although the B-site cation primarily impacts these metrics, the A-cation imparts a secondary effect. FA-only compositions with 50 or 60% Sn, displayed an order of magnitude lower initial conductivity values than their FA/MA and FA/Cs counterparts, which suggests that they have oxidized to a lesser degree by the time of measurement. While the data presented in Figure 4a for the 50% Sn composition, indicates that the FA/MA films have a shorter characteristic oxidation time than FA and FA/Cs, the error bars are such that these values are statistically indistinguishable. Therefore, of the films investigated, we conclude that the $FAPb_{0.5}Sn_{0.5}I_3$ composition is the least likely to be oxidized during preparation and within the few minutes of handling in air. However, the rate of degradation by oxidation is very similar between the A-site compositions considered.

Discussion

The main goal of this work is to identify which front-leading low bandgap Pb-Sn composition would be the most suitable to serve as the baseline absorber material upon which subsequent research and development would proceed in an industrial setting. High efficiency and long operational lifetime are key requirements for the commercialization of any solar cell technology, therefore identifying the main risks that threaten device stability is critical for material selection, process development, and product design. In industrial research and development programs, the process of device development must be methodical and intentional in order to make efficient use of resources and meet key milestones. Therefore, it is crucial that we select as the starting point for further development an absorber composition that avoids irreversible degradation processes as much as possible and then design the rest of the device around it, for instance by selecting contacts for optimal energetic alignment, chemical compatibility, and deposition methodology. Ultimately, full device reliability assessment by standard accelerated stress testing will determine the operational stability of the solar product. But we expect that these core degradation modes identified for the bulk absorber will still be relevant and must be considered far upstream in the development process.

To summarize our findings, we identified three irreversible degradation processes in narrow band gap Pb-Sn perovskite absorbers: (1) Sn oxidation upon air exposure, (2) MA loss upon heat exposure, and (3) FA/Cs segregation leading to impurity phase formation. In light of these absorber degradation modes, we present a schematic in Figure 5a that filters the candidate A-site compositions down to those that are practically de-risked for further development in an industrial setting. (1) It is clear that the optoelectronic quality of all Pb-Sn perovskites, regardless of A-site composition, rapidly degrades on the order of 30 minutes upon air exposure due to the irreversible reaction of O_2 with the Sn^{2+}. This highlights that commercial solar cells employing these materials will require robust encapsulation to ensure that air exposure is minimized during their operational lifetime. However, it would be uneconomical and impractical in an industrial setting to completely avoid any air exposure during manufacturing. Therefore, the most appropriate composition would need to tolerate some air exposure before encapsulation proceeds. We find that the initial conductivity decreases with decreasing Sn content, thereby indicating a less oxidized state at the time of measurement in air. Therefore, we select the 50% Sn compositions for further consideration because they would better tolerate small doses of atmosphere that are likely to occur in a production line, while still maintaining a suitably low bandgap. (2) We confirm the findings of other reports [51,53,54] that MA loss occurs upon heating at 100°C and leads to the decomposition of the perovskite absorber and the generation

of PbI_2. Although solar cells deployed in terrestrial applications will see maximum temperatures of only 60-70°C [69], in space applications the temperature can exceed 100°C. [70,71] Encouragingly, there are reports of MA-based neat Pb-perovskites devices performing well after elevated temperature stressing at 85°C [72] and triple-cation perovskites maintaining high performance in outdoor testing. [73] However, from a practical perspective, the MA-loss mechanism still poses a risk that over the course of decades-long operation some degree of absorber degradation occurs, whereas FA and FA/Cs compositions show improved thermal stability. Furthermore, accelerated stress testing at elevated temperatures, such as damp heat testing at 85°C, is standard for the industry at this time and ensuring robustness against such tests is important for early commercialization of perovskite technology. By this rationale, we withdraw MA-based compositions from further consideration. (3) We have observed that FA and Cs can segregate from the perovskite lattice upon air exposure and leads to the formation of the non-perovskite δ-$CsPbI_3$ phase. Our DFT calculations have highlighted that oxygen prefers to interact with FA and Sn, thereby providing a potential impetus for A-cation de-mixing that explains our observations. It could be argued that this mechanism is inconsequential since we observe it only upon air exposure, which will have already degraded the optoelectronic quality to the point of being unusable anyway. However, from a conservative standpoint of de-risking future investment in the technology, any benefits associated from mixing FA/Cs at the A-site would have to outweigh the potential for this mechanism to become activated by either minor air exposure or perhaps a separate stressor. [74,75] In neat Pb perovskite compositions, the perovskite phase of $FAPbI_3$ is inherently unstable and requires the addition of other cations, most traditionally MA or Cs, to preserve the 3D corner-sharing octahedral network required for efficient photovoltaic operation. However, it is important to note that the narrow bandgap $FA(Sn_yPb_{1-y})I_3$ compositions considered here do not show sign of such phase instability, although it is not yet understood why given the smaller cavity formed by the Pb-Sn octahedra. Rather, they nucleate directly into the alpha-phase upon solvent quenching and our XRD study has not shown any indication of the non-perovskite delta-phase formation during thermal or atmospheric stressing. This then leads us to conclude that of the nine compositions considered in this study, the $FASn_{0.5}Pb_{0.5}I_3$ is the most likely to avoid the irreversible absorber degradation processes that we identify.

Although $FASn_{0.5}Pb_{0.5}I_3$ was one of the first low-bandgap perovskite absorber materials to be integrated into all-perovskite tandems [76], it has seen relatively little development compared with FA/Cs, FA/MA, and triple-cation compositions. While we have argued that $FASn_{0.5}Pb_{0.5}I_3$ can help minimize risk of material destabilization, it must also offer competitive photovoltaic performances. To demonstrate that it is indeed capable of this, we constructed single-junction devices from both $FASn_{0.5}Pb_{0.5}I_3$ and $FA_{0.75}Cs_{0.25}Sn_{0.5}Pb_{0.5}I_3$ with 1 cm^2 device areas using the same fabrication procedure and device stack. [62] Figure 5b shows that we achieve statistically indistinguishable power conversion efficiency distributions with mean performance around 12.5% and champions near 14% for both compositions. From our judgement, the inclusion of Cs in the formulation does not confer any obvious benefit to the performance under the conditions trialled.

Nevertheless, even with the judicious selection of absorber composition, oxidation remains a critical concern for these materials and a means to quantify and monitor this process is required for assessing absorber development and product encapsulation. We have already shown how long-range conductivity is sensitive enough to detect even minor oxidation and provides high enough dynamic range to monitor the process over 7 orders of magnitude. To demonstrate this, we show in Figure 5c the conductivity profile of companion perovskite films that are either exposed directly to air, capped with a polymethyl methacrylate (PMMA) layer, or encapsulated by a cover glass. When encapsulated with glass, we find that the conductivity remains constant even after hours of exposure. This simultaneously proves that air exposure is responsible for the conductivity behaviour we observe and

that the process can be practically managed with careful encapsulation. In contrast, the PMMA-capped material shows a slowed initial increase that sharply transitions to the characteristic profile after a certain amount of time. We attribute this new feature to the oxidation process being delayed by the PMMA capping layer, which initially causes the reaction to become diffusion-limited until it becomes fully saturated with air. It is also noteworthy that PMMA is hydrophobic and oxygen permeable, which supports our assumption that oxygen is primarily responsible for the oxidation process monitored by conductivity rather than water.

Conclusion

In this study, we assessed the thermal and atmospheric stability of a set of nine low bandgap perovskite compositions using both widely accessible and advanced characterization techniques. By identifying irreversible degradation processes that can arise from the choice of A- and B-site composition, we propose that $FASn_{0.5}Pb_{0.5}I_3$ is the least susceptible to bulk degradation modes that could arise through inevitable heat and atmosphere exposure that will occur during solar cell manufacture and operation. Of those investigated systems, this composition is more thermally stable and demonstrates better initial oxidation resistance than the mixed A-site compositions. We further show that it is capable of achieving good photovoltaic performance when incorporated in 1 cm^2 devices that is statistically identical to the companion devices made with the front-running FA/Cs composition. From the perspective of industrial development towards commercializing a product, we consider the $FA(Sn_{0.5}Pb_{0.5})I_3$ composition to be an ideal platform from which improvements can be introduced and device architectures can be designed for maximizing performance and lifetime. We further propose using long-range conductivity as a characterization method to quantify the oxidative process; this approach enables practical assessment of both absorbers with improved oxidative resistance and the effectiveness of encapsulation robustness that will be required for commercial all-perovskite multijunction products.

Acknowledgements

C.K. would like to acknowledge funding from the European Union's Horizon 2020 Framework Program for funding Research and Innovation under Grant Agreement No. 764787 (MAESTRO). Acknowledgement: V.J.Y.L thanks Oxford Photovoltaics for funding his studentship, and the Rank Prize for a Return to Research grant. L.M.H. thanks TUM-IAS for a Hans Fischer Senior Fellowship and Award. N.Z and M.S.I thank the HEC Materials Chemistry Consortium (EP/R029431/1) for Archer supercomputer facilities.

Conflicts of Interests

C.K, M.T.K, L.M.P and C.C are employees at Oxford Photovoltaics, Ltd.

Data availability

The data that support the findings of this study are available from the corresponding author upon reasonable request.

Figures

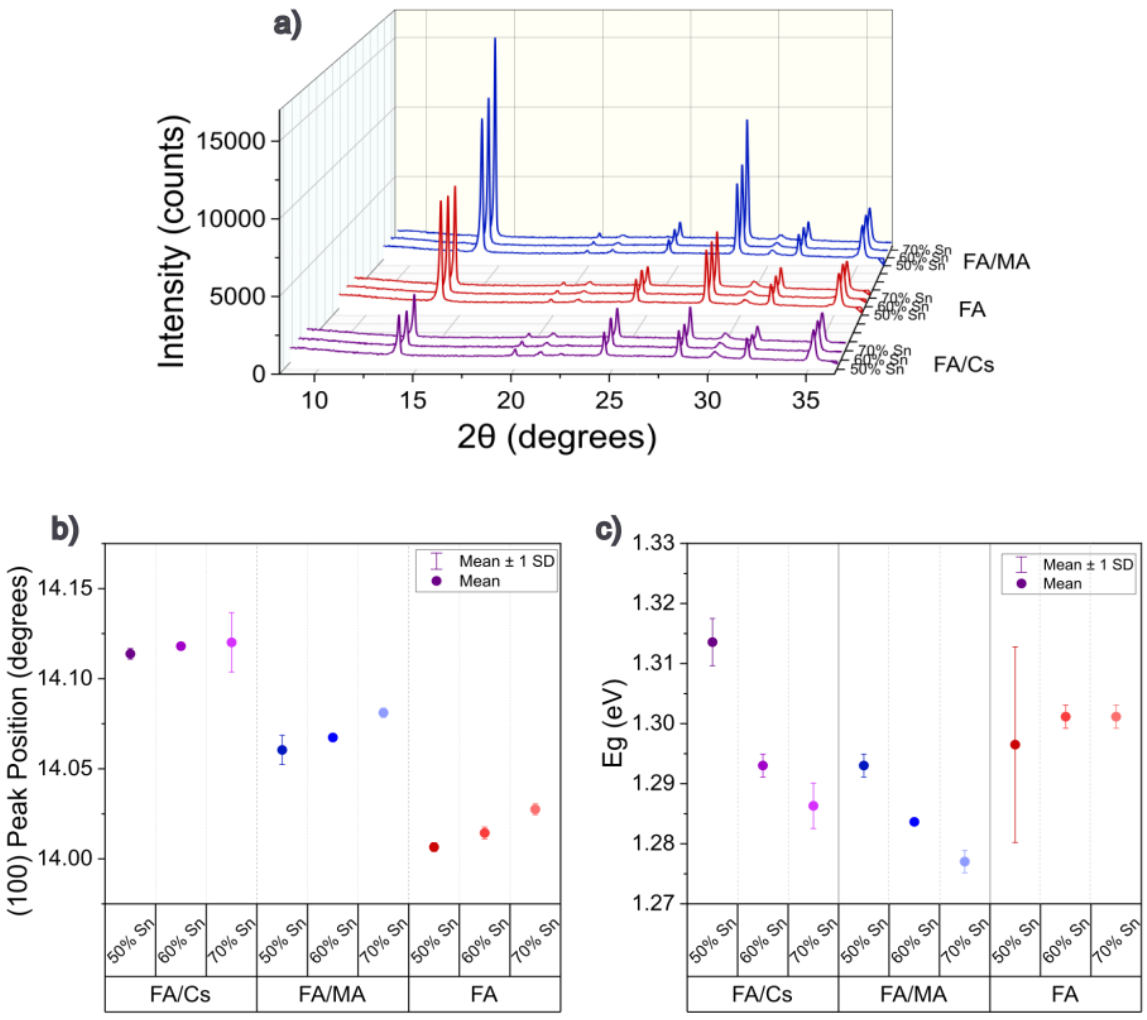

Figure 1: a) X-ray diffraction patterns, b) (100) perovskite peak position and c) bandgap values for thin films of $FA_{0.75}Cs_{0.25}Sn_xPb_{1-x}I_3$ (purple), $FASn_xPb_{1-x}I_3$ (red) and $FA_{0.6}MA_{0.4}Sn_xPb_{1-x}I_3$ (blue) for x=0.5,0.6, 0.7

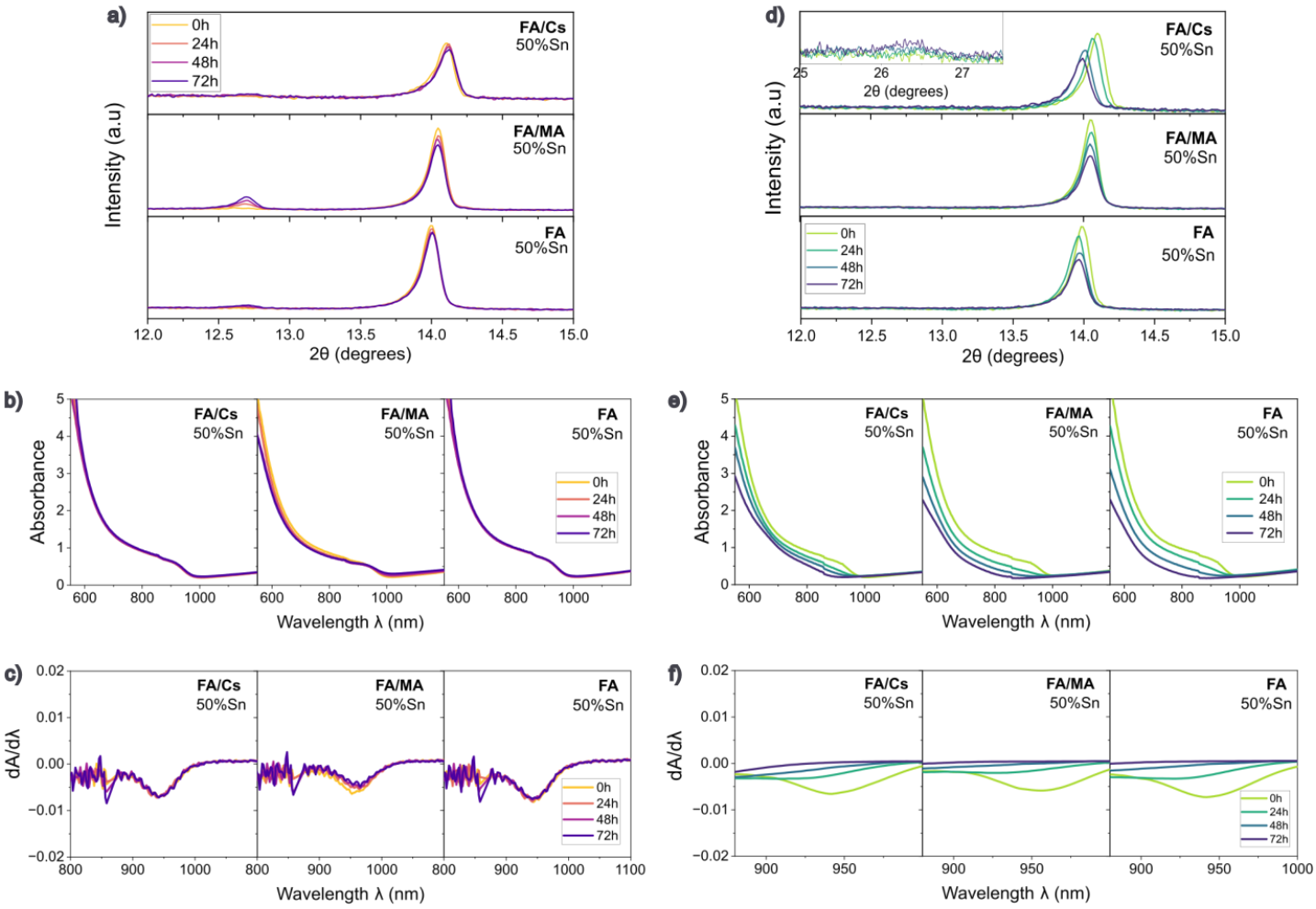

Figure 2: (a,c) Evolution of XRD patterns during (a) heat stressing at 100°C in N_2 atmosphere (red gradient) and (c) air exposure at room temperature (blue gradient) for $FA_{0.75}Cs_{0.25}Sn_{0.5}Pb_{0.5}I_3$, $FASn_{0.5}Pb_{0.5}I_3$ and $FA_{0.6}MA_{0.4}Sn_{0.5}Pb_{0.5}I_3$ thin films. (b,d) Evolution of absorption spectra and first derivative peak corresponding to bandgap edge during (b) heat stressing at 100°C in N_2 atmosphere (red gradient) and (d) air exposure at room temperature (blue gradient) for $FA_{0.75}Cs_{0.25}Sn_{0.5}Pb_{0.5}I_3$, $FASn_{0.5}Pb_{0.5}I_3$ and $FA_{0.6}MA_{0.4}Sn_{0.5}Pb_{0.5}I_3$ thin films. Measurements were taken after 24, 48 and 72 hours of stressing.

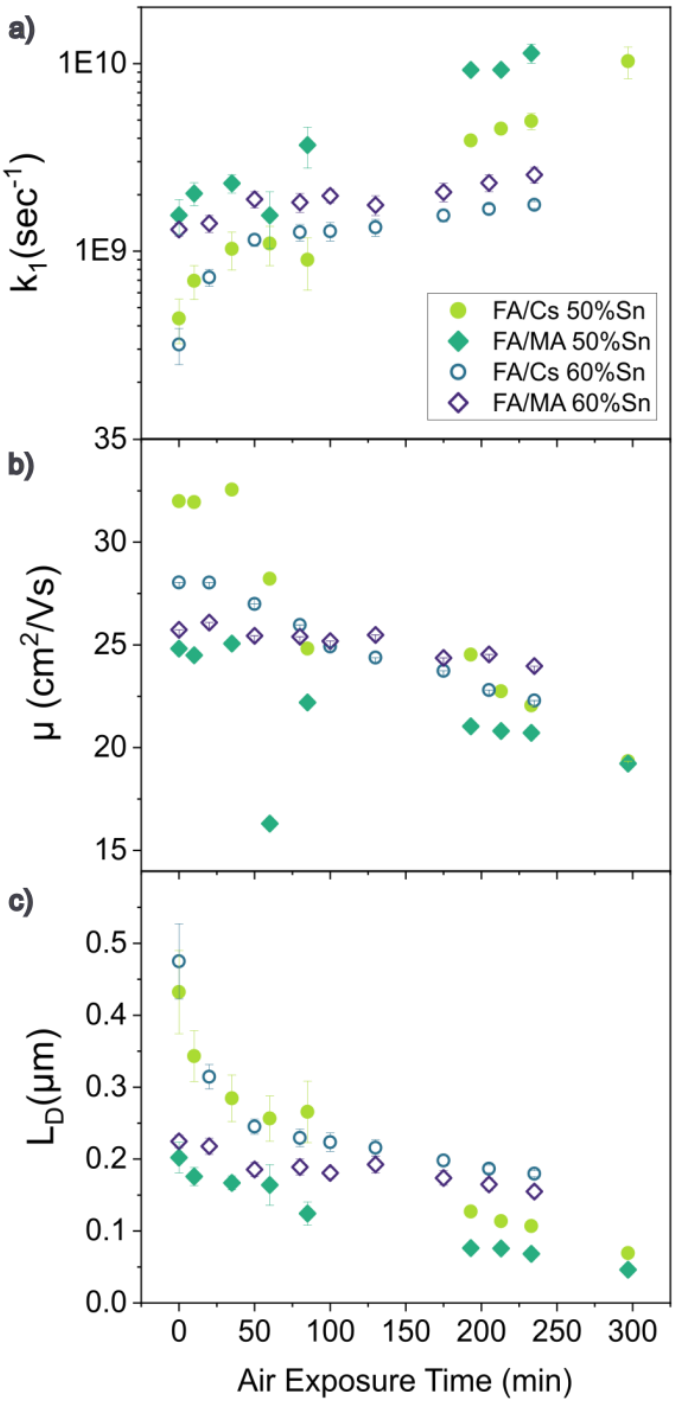

Figure 3: a) Monomolecular charge-carrier recombination rates (k_1), b) charge-carrier sum mobilities (μ) and c) charge-carrier diffusion lengths (L_D) of mixed lead-tin perovskites with the compositions indicated in the legend at discrete air-exposure times, obtained from optical-pump THz-probe photoconductivity measurements performed with 400 nm wavelength photoexcitation, as detailed in the respective section of the SI. Photoconductivity decay transients from which these values are extracted are shown in Figure S1-S4 in the SI.

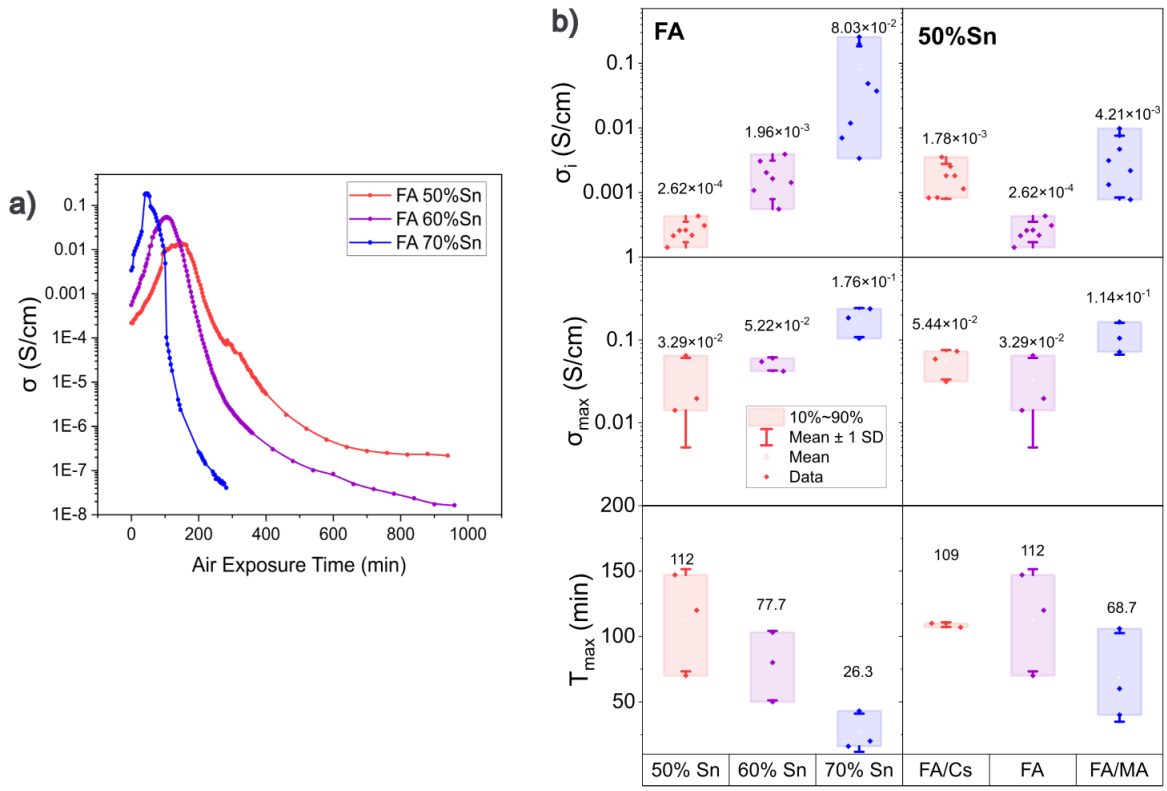

Figure 4: a) Lateral conductivity as a function of air exposure time at room temperature for $FASn_xPb_{1-x}I_3$ (x=0.4, 0.5 and 0.6) (lines are used as guide for the eye) and (b) distributions of initial conductivity values (σ_i) maximum conductivity values (σ_{max}) and time needed to reach the maximum value(T_{max}) for $FASn_xPb_{1-x}I_3$ (x=0.4,0.5 and 0.6) (panel (a)) and $ASn_{0.5}Pb_{0.5}I_3$ ($A=FA_{0.75}Cs_{0.25}$, FA and $FA_{0.6}MA_{0.4}$) (panel (b)).

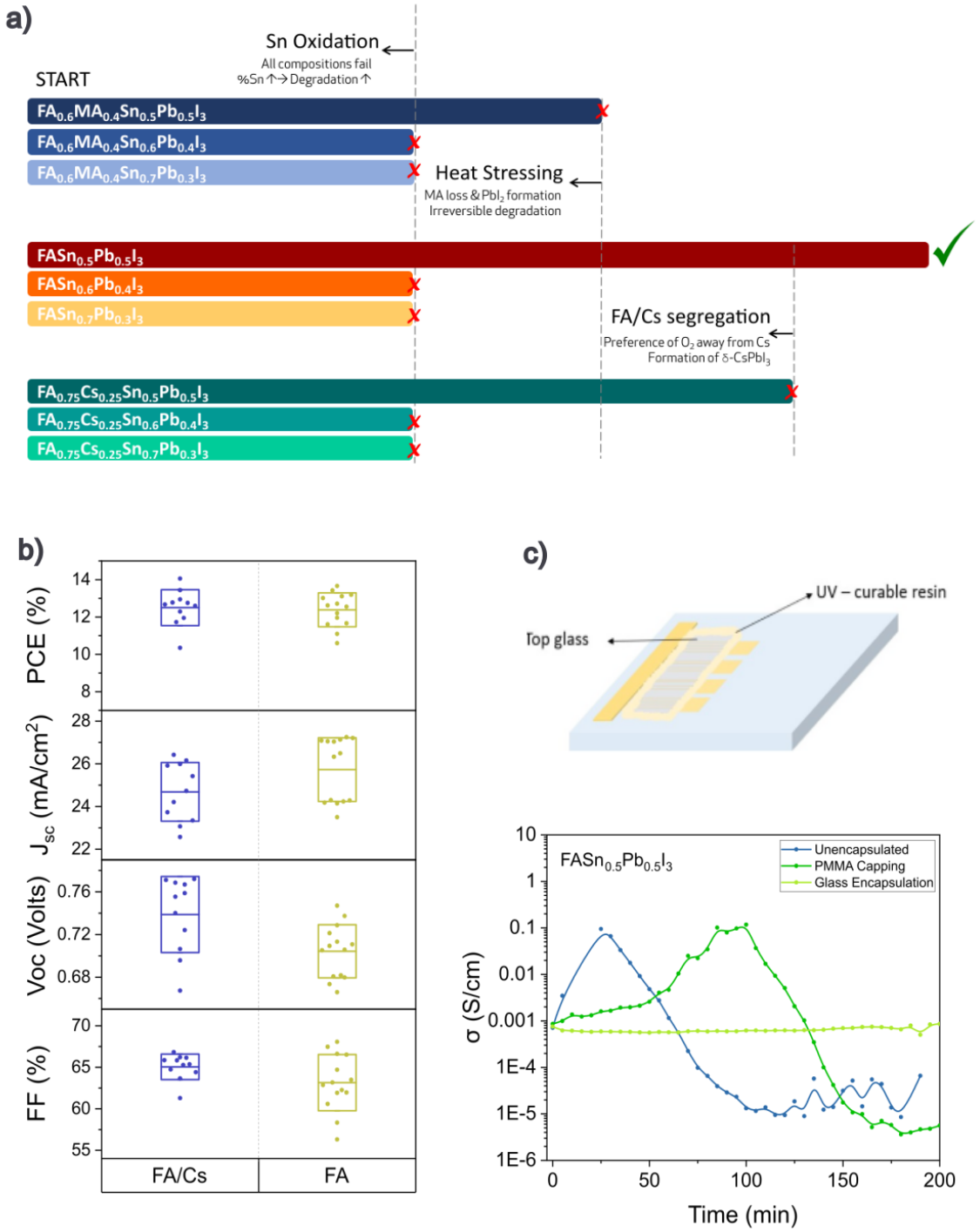

Figure 5: a) Schematic chart filtering the candidate low-bandgap compositions $APb_xSn_{1-x}I_3$ (A= $FA_{0.75}Cs_{0.25}$, FA and $FA_{0.6}MA_{0.4}$, x=0.3,0.4 or 0.5), (b) power conversion efficiency (PCE), short-circuit current density (J_{SC}), open-circuit voltage (V_{OC}) and fill factor (FF) values of $FA_{0.75}Cs_{0.25}Pb_{0.5}Sn_{0.5}I_3$ (blue) and $FASn_{0.5}Pb_{0.5}I_3$ (green) devices. (C) Schematic representation of encapsulated conductivity samples and real-time lateral conductivity profiles of unencapsulated (blue), PMMA capped (green) and encapsulated (yellow) $FASn_{0.5}Pb_{0.5}I_3$ samples.

References

[1] Oxford PV sets new solar cell world record | Oxford PV, (n.d.). https://www.oxfordpv.com/news/oxford-pv-sets-new-solar-cell-world-record (accessed August 22, 2023).

[2] NREL Efficiency Chart, (n.d.). https://www.nrel.gov/pv/cell-efficiency.html (accessed October 26, 2022).

[3] Best Research-Cell Efficiency Chart. U.S. National Renewable Energy Laboratory. https://www.nrel.gov/pv/cell-efficiency.html, 2021. https://www.nrel.gov/pv/cell-efficiency.html.

[4] M. Fischer, International Technology Roadmap for Photovoltaic (ITRPV) 11th edition, April 2020, International Technology Roadmap for Photovoltaic (ITRPV) 11th Edition, April 2020. (2019) 41.

[5] R. He, W. Wang, Z. Yi, F. Lang, C. Chen, J. Luo, J. Zhu, J. Thiesbrummel, S. Shah, K. Wei, Y. Luo, C. Wang, H. Lai, H. Huang, J. Zhou, B. Zou, X. Yin, S. Ren, X. Hao, L. Wu, J. Zhang, J. Zhang, M. Stolterfoht, F. Fu, W. Tang, D. Zhao, All-perovskite tandem 1 cm2 cells with improved interface quality, Nature. (2023) 1–3. https://doi.org/10.1038/s41586-023-05992-y.

[6] R. Lin, Y. Wang, Q. Lu, B. Tang, J. Li, H. Gao, Y. Gao, H. Li, C. Ding, J. Wen, P. Wu, C. Liu, S. Zhao, K. Xiao, Z. Liu, C. Ma, Y. Deng, L. Li, F. Fan, H. Tan, All-perovskite tandem solar cells with 3D/3D bilayer perovskite heterojunction, Nature. 620 (2023) 994–1000. https://doi.org/10.1038/s41586-023-06278-z.

[7] Z. Yang, Z. Yu, H. Wei, X. Xiao, Z. Ni, B. Chen, Y. Deng, S.N. Habisreutinger, X. Chen, K. Wang, J. Zhao, P.N. Rudd, J.J. Berry, M.C. Beard, J. Huang, Enhancing electron diffusion length in narrow-bandgap perovskites for efficient monolithic perovskite tandem solar cells, Nat Commun. 10 (2019) 4498. https://doi.org/10.1038/s41467-019-12513-x.

[8] K. Xiao, R. Lin, Q. Han, Y. Hou, Z. Qin, H.T. Nguyen, J. Wen, M. Wei, V. Yeddu, M.I. Saidaminov, Y. Gao, X. Luo, Y. Wang, H. Gao, C. Zhang, J. Xu, J. Zhu, E.H. Sargent, H. Tan, All-perovskite tandem solar cells with 24.2% certified efficiency and area over 1 cm2 using surface-anchoring zwitterionic antioxidant, Nat Energy. 5 (2020) 870–880. https://doi.org/10.1038/s41560-020-00705-5.

[9] J. Tong, Z. Song, D.H. Kim, X. Chen, C. Chen, A.F. Palmstrom, P.F. Ndione, M.O. Reese, S.P. Dunfield, O.G. Reid, J. Liu, F. Zhang, S.P. Harvey, Z. Li, S.T. Christensen, G. Teeter, D. Zhao, M.M. Al-Jassim, M.F.A.M. van Hest, M.C. Beard, S.E. Shaheen, J.J. Berry, Y. Yan, K. Zhu, Carrier lifetimes of >1 μs in Sn-Pb perovskites enable efficient all-perovskite tandem solar cells, Science. 364 (2019) 475–479. https://doi.org/10.1126/science.aav7911.

[10] C. Li, Z. Song, C. Chen, C. Xiao, B. Subedi, S.P. Harvey, N. Shrestha, K.K. Subedi, L. Chen, D. Liu, Y. Li, Y.-W. Kim, C. Jiang, M.J. Heben, D. Zhao, R.J. Ellingson, N.J. Podraza, M. Al-Jassim, Y. Yan, Low-bandgap mixed tin–lead iodide perovskites with reduced methylammonium for simultaneous enhancement of solar cell efficiency and stability, Nat Energy. 5 (2020) 768–776. https://doi.org/10.1038/s41560-020-00692-7.

[11] G. Kapil, T. Bessho, T. Maekawa, A.K. Baranwal, Y. Zhang, M.A. Kamarudin, D. Hirotani, Q. Shen, H. Segawa, S. Hayase, Tin-Lead Perovskite Fabricated via Ethylenediamine Interlayer Guides to the Solar Cell Efficiency of 21.74%, Advanced Energy Materials. n/a (n.d.) 2101069. https://doi.org/10.1002/aenm.202101069.

[12] R. Prasanna, T. Leijtens, S.P. Dunfield, J.A. Raiford, E.J. Wolf, S.A. Swifter, J. Werner, G.E. Eperon, C. de Paula, A.F. Palmstrom, C.C. Boyd, M.F.A.M. van Hest, S.F. Bent, G. Teeter, J.J. Berry, M.D. McGehee, Design of low bandgap tin–lead halide perovskite solar cells to achieve thermal, atmospheric and operational stability, Nature Energy. 4 (2019) 939–947. https://doi.org/10.1038/s41560-019-0471-6.

[13] T. Chen, B.J. Foley, C. Park, C.M. Brown, L.W. Harriger, J. Lee, J. Ruff, M. Yoon, J.J. Choi, S.-H. Lee, Entropy-driven structural transition and kinetic trapping in formamidinium lead iodide perovskite, Science Advances. 2 (2016) e1601650. https://doi.org/10.1126/sciadv.1601650.
[14] P. Gratia, I. Zimmermann, P. Schouwink, J.-H. Yum, J.-N. Audinot, K. Sivula, T. Wirtz, M.K. Nazeeruddin, The Many Faces of Mixed Ion Perovskites: Unraveling and Understanding the Crystallization Process, ACS Energy Lett. 2 (2017) 2686–2693. https://doi.org/10.1021/acsenergylett.7b00981.
[15] M.T. Weller, O.J. Weber, J.M. Frost, A. Walsh, Cubic Perovskite Structure of Black Formamidinium Lead Iodide, α-[HC(NH2)2]PbI3, at 298 K, J. Phys. Chem. Lett. 6 (2015) 3209–3212. https://doi.org/10.1021/acs.jpclett.5b01432.
[16] N.J. Jeon, J.H. Noh, W.S. Yang, Y.C. Kim, S. Ryu, J. Seo, S.I. Seok, Compositional engineering of perovskite materials for high-performance solar cells, Nature. 517 (2015) 476–480. https://doi.org/10.1038/nature14133.
[17] N. Pellet, P. Gao, G. Gregori, T.-Y. Yang, M.K. Nazeeruddin, J. Maier, M. Grätzel, Mixed-Organic-Cation Perovskite Photovoltaics for Enhanced Solar-Light Harvesting, Angewandte Chemie International Edition. 53 (2014) 3151–3157. https://doi.org/10.1002/anie.201309361.
[18] D.P. McMeekin, G. Sadoughi, W. Rehman, G.E. Eperon, M. Saliba, M.T. Hörantner, A. Haghighirad, N. Sakai, L. Korte, B. Rech, M.B. Johnston, L.M. Herz, H.J. Snaith, A mixed-cation lead mixed-halide perovskite absorber for tandem solar cells, Science. 351 (2016) 151 LP – 155.
[19] M. Saliba, T. Matsui, J.-Y. Seo, K. Domanski, J.-P. Correa-Baena, M.K. Nazeeruddin, S.M. Zakeeruddin, W. Tress, A. Abate, A. Hagfeldt, M. Grätzel, Cesium-containing triple cation perovskite solar cells: improved stability, reproducibility and high efficiency, Energy Environ. Sci. 9 (2016) 1989–1997. https://doi.org/10.1039/C5EE03874J.
[20] H. Min, M. Kim, S.-U. Lee, H. Kim, G. Kim, K. Choi, J.H. Lee, S.I. Seok, Efficient, stable solar cells by using inherent bandgap of α-phase formamidinium lead iodide, Science. 366 (2019) 749–753. https://doi.org/10.1126/science.aay7044.
[21] G. Kim, H. Min, K.S. Lee, D.Y. Lee, S.M. Yoon, S.I. Seok, Impact of strain relaxation on performance of α-formamidinium lead iodide perovskite solar cells, Science. (2020). https://doi.org/10.1126/science.abc4417.
[22] J.-W. Lee, D.-H. Kim, H.-S. Kim, S.-W. Seo, S.M. Cho, N.-G. Park, Formamidinium and Cesium Hybridization for Photo- and Moisture-Stable Perovskite Solar Cell, Advanced Energy Materials. 5 (2015) 1501310. https://doi.org/10.1002/aenm.201501310.
[23] S. Tan, I. Yavuz, N. De Marco, T. Huang, S.-J. Lee, C.S. Choi, M. Wang, S. Nuryyeva, R. Wang, Y. Zhao, H.-C. Wang, T.-H. Han, B. Dunn, Y. Huang, J.-W. Lee, Y. Yang, Steric Impediment of Ion Migration Contributes to Improved Operational Stability of Perovskite Solar Cells, Advanced Materials. 32 (2020) 1906995. https://doi.org/10.1002/adma.201906995.
[24] E. Mosconi, F. De Angelis, Mobile Ions in Organohalide Perovskites: Interplay of Electronic Structure and Dynamics, ACS Energy Lett. 1 (2016) 182–188. https://doi.org/10.1021/acsenergylett.6b00108.
[25] A. Senocrate, I. Spanopoulos, N. Zibouche, J. Maier, M.S. Islam, M.G. Kanatzidis, Tuning Ionic and Electronic Conductivities in the “Hollow” Perovskite {en}MAPbI3, Chem. Mater. 33 (2021) 719–726. https://doi.org/10.1021/acs.chemmater.0c04139.
[26] D.W. Ferdani, S.R. Pering, D. Ghosh, P. Kubiak, A.B. Walker, S.E. Lewis, A.L. Johnson, P.J. Baker, M.S. Islam, P.J. Cameron, Partial cation substitution reduces iodide ion transport in lead iodide perovskite solar cells, Energy Environ. Sci. 12 (2019) 2264–2272. https://doi.org/10.1039/C9EE00476A.
[27] A.J. Knight, J. Borchert, R.D.J. Oliver, J.B. Patel, P.G. Radaelli, H.J. Snaith, M.B. Johnston, L.M. Herz, Halide Segregation in Mixed-Halide Perovskites: Influence of A-Site Cations, ACS Energy Lett. 6 (2021) 799–808. https://doi.org/10.1021/acsenergylett.0c02475.
[28] J.-P. Correa-Baena, Y. Luo, T.M. Brenner, J. Snaider, S. Sun, X. Li, M.A. Jensen, N.T.P. Hartono, L. Nienhaus, S. Wieghold, J.R. Poindexter, S. Wang, Y.S. Meng, T. Wang, B. Lai, M.V. Holt, Z. Cai,

M.G. Bawendi, L. Huang, T. Buonassisi, D.P. Fenning, Homogenized halides and alkali cation segregation in alloyed organic-inorganic perovskites, Science. 363 (2019) 627–631. https://doi.org/10.1126/science.aah5065.

[29] H.X. Dang, K. Wang, M. Ghasemi, M.-C. Tang, M. De Bastiani, E. Aydin, E. Dauzon, D. Barrit, J. Peng, D.-M. Smilgies, S. De Wolf, A. Amassian, Multi-cation Synergy Suppresses Phase Segregation in Mixed-Halide Perovskites, Joule. 3 (2019) 1746–1764. https://doi.org/10.1016/j.joule.2019.05.016.

[30] D. Ghosh, A.R. Smith, A.B. Walker, M.S. Islam, Mixed A-Cation Perovskites for Solar Cells: Atomic-Scale Insights Into Structural Distortion, Hydrogen Bonding, and Electronic Properties, Chem. Mater. 30 (2018) 5194–5204. https://doi.org/10.1021/acs.chemmater.8b01851.

[31] Mechanism of Pressure-Induced Phase Transitions, Amorphization, and Absorption-Edge Shift in Photovoltaic Methylammonium Lead Iodide | The Journal of Physical Chemistry Letters, (n.d.). https://pubs.acs.org/doi/full/10.1021/acs.jpclett.6b01648 (accessed May 26, 2023).

[32] R. Prasanna, A. Gold-Parker, T. Leijtens, B. Conings, A. Babayigit, H.-G. Boyen, M.F. Toney, M.D. McGehee, Band Gap Tuning via Lattice Contraction and Octahedral Tilting in Perovskite Materials for Photovoltaics, J. Am. Chem. Soc. 139 (2017) 11117–11124. https://doi.org/10.1021/jacs.7b04981.

[33] F. El-Mellouhi, A. Marzouk, E.T. Bentria, S.N. Rashkeev, S. Kais, F.H. Alharbi, Hydrogen Bonding and Stability of Hybrid Organic–Inorganic Perovskites, ChemSusChem. 9 (2016) 2648–2655. https://doi.org/10.1002/cssc.201600864.

[34] R.M. Dos Santos, I. Ornelas−Cruz, A.C. Dias, M.P. Lima, J.L.F. Da Silva, Theoretical Investigation of the Role of Mixed A^{+} Cations in the Structure, Stability, and Electronic Properties of Perovskite Alloys, ACS Appl. Energy Mater. 6 (2023) 5259–5273. https://doi.org/10.1021/acsaem.3c00186.

[35] K.T. Munson, J.R. Swartzfager, J. Gan, J.B. Asbury, Does Dipolar Motion of Organic Cations Affect Polaron Dynamics and Bimolecular Recombination in Halide Perovskites?, J. Phys. Chem. Lett. 11 (2020) 3166–3172. https://doi.org/10.1021/acs.jpclett.0c00762.

[36] L. Zhou, C. Katan, W. Nie, H. Tsai, L. Pedesseau, J.J. Crochet, J. Even, A.D. Mohite, S. Tretiak, A.J. Neukirch, Cation Alloying Delocalizes Polarons in Lead Halide Perovskites, J. Phys. Chem. Lett. 10 (2019) 3516–3524. https://doi.org/10.1021/acs.jpclett.9b01077.

[37] L.R.V. Buizza, L.M. Herz, Polarons and Charge Localization in Metal-Halide Semiconductors for Photovoltaic and Light-Emitting Devices, Advanced Materials. n/a (n.d.) 2007057. https://doi.org/10.1002/adma.202007057.

[38] Z. Wang, Q. Lin, F.P. Chmiel, N. Sakai, L.M. Herz, H.J. Snaith, Efficient ambient-air-stable solar cells with 2D–3D heterostructured butylammonium-caesium-formamidinium lead halide perovskites, Nat Energy. 2 (2017) 1–10. https://doi.org/10.1038/nenergy.2017.135.

[39] G. Grancini, C. Roldán-Carmona, I. Zimmermann, E. Mosconi, X. Lee, D. Martineau, S. Narbey, F. Oswald, F. De Angelis, M. Graetzel, M.K. Nazeeruddin, One-Year stable perovskite solar cells by 2D/3D interface engineering, Nature Communications. 8 (2017) 15684. https://doi.org/10.1038/ncomms15684.

[40] K.P. Marshall, M. Walker, R.I. Walton, R.A. Hatton, Enhanced stability and efficiency in hole-transport-layer-free CsSnI3 perovskite photovoltaics, Nat Energy. 1 (2016) 1–9. https://doi.org/10.1038/nenergy.2016.178.

[41] C.C. Stoumpos, C.D. Malliakas, M.G. Kanatzidis, Semiconducting Tin and Lead Iodide Perovskites with Organic Cations: Phase Transitions, High Mobilities, and Near-Infrared Photoluminescent Properties, Inorg. Chem. 52 (2013) 9019–9038. https://doi.org/10.1021/ic401215x.

[42] S.J. Lee, S.S. Shin, Y.C. Kim, D. Kim, T.K. Ahn, J.H. Noh, J. Seo, S.I. Seok, Fabrication of Efficient Formamidinium Tin Iodide Perovskite Solar Cells through SnF_2-Pyrazine Complex, J Am Chem Soc. 138 (2016) 3974–3977. https://doi.org/10.1021/jacs.6b00142.

[43] L. Lanzetta, T. Webb, N. Zibouche, X. Liang, D. Ding, G. Min, R.J.E. Westbrook, B. Gaggio, T.J. Macdonald, M.S. Islam, S.A. Haque, Degradation mechanism of hybrid tin-based perovskite solar cells and the critical role of tin (IV) iodide, Nat Commun. 12 (2021) 2853. https://doi.org/10.1038/s41467-021-22864-z.
[44] S. Gupta, D. Cahen, G. Hodes, How SnF2 Impacts the Material Properties of Lead-Free Tin Perovskites, J. Phys. Chem. C. 122 (2018) 13926–13936. https://doi.org/10.1021/acs.jpcc.8b01045.
[45] I. Chung, B. Lee, J. He, R.P.H. Chang, M.G. Kanatzidis, All-solid-state dye-sensitized solar cells with high efficiency, Nature. 485 (2012) 486–489. https://doi.org/10.1038/nature11067.
[46] J.H. Heo, J. Kim, H. Kim, S.H. Moon, S.H. Im, K.-H. Hong, Roles of SnX2 (X = F, Cl, Br) Additives in Tin-Based Halide Perovskites toward Highly Efficient and Stable Lead-Free Perovskite Solar Cells, J. Phys. Chem. Lett. 9 (2018) 6024–6031. https://doi.org/10.1021/acs.jpclett.8b02555.
[47] J. Pascual, M. Flatken, R. Félix, G. Li, S.-H. Turren-Cruz, M.H. Aldamasy, C. Hartmann, M. Li, D.D. Girolamo, G. Nasti, E. Hüsam, R.G. Wilks, A. Dallmann, M. Bär, A. Hoell, A. Abate, Fluoride Chemistry in Tin Halide Perovskites, Angewandte Chemie International Edition. n/a (n.d.). https://doi.org/10.1002/anie.202107599.
[48] R. Lin, K. Xiao, Z. Qin, Q. Han, C. Zhang, M. Wei, M.I. Saidaminov, Y. Gao, J. Xu, M. Xiao, A. Li, J. Zhu, E.H. Sargent, H. Tan, Monolithic all-perovskite tandem solar cells with 24.8% efficiency exploiting comproportionation to suppress Sn(II) oxidation in precursor ink, Nat Energy. 4 (2019) 864–873. https://doi.org/10.1038/s41560-019-0466-3.
[49] W. Travis, E.N.K. Glover, H. Bronstein, D.O. Scanlon, R.G. Palgrave, On the application of the tolerance factor to inorganic and hybrid halide perovskites: a revised system, Chemical Science. 7 (2016) 4548–4556. https://doi.org/10.1039/C5SC04845A.
[50] M.T. Hörantner, T. Leijtens, M.E. Ziffer, G.E. Eperon, M.G. Christoforo, M.D. McGehee, H.J. Snaith, The Potential of Multijunction Perovskite Solar Cells, ACS Energy Lett. 2 (2017) 2506–2513. https://doi.org/10.1021/acsenergylett.7b00647.
[51] B. Conings, J. Drijkoningen, N. Gauquelin, A. Babayigit, J. D'Haen, L. D'Olieslaeger, A. Ethirajan, J. Verbeeck, J. Manca, E. Mosconi, F.D. Angelis, H. Boyen, Intrinsic Thermal Instability of Methylammonium Lead Trihalide Perovskite, Advanced Energy Materials. (2015) 1–8. https://doi.org/10.1002/aenm.201500477.
[52] T.T. Ava, A. Al Mamun, S. Marsillac, G. Namkoong, A Review: Thermal Stability of Methylammonium Lead Halide Based Perovskite Solar Cells, Applied Sciences. 9 (2019) 188. https://doi.org/10.3390/app9010188.
[53] B. Brunetti, C. Cavallo, A. Ciccioli, G. Gigli, A. Latini, On the Thermal and Thermodynamic (In)Stability of Methylammonium Lead Halide Perovskites, Sci Rep. 6 (2016) 31896. https://doi.org/10.1038/srep31896.
[54] E.J. Juarez-Perez, L.K. Ono, M. Maeda, Y. Jiang, Z. Hawash, Y. Qi, Photodecomposition and thermal decomposition in methylammonium halide lead perovskites and inferred design principles to increase photovoltaic device stability, J. Mater. Chem. A. 6 (2018) 9604–9612. https://doi.org/10.1039/C8TA03501F.
[55] J. Yang, B.D. Siempelkamp, D. Liu, T.L. Kelly, An Investigation of CH 3 NH 3 PbI 3 Degradation Rates and Mechanisms in Controlled Humidity Environments Using in situ Techniques, ACS Nano. 9 (2015) 1955–1963. https://doi.org/10.1021/nn506864k.
[56] T. Leijtens, R. Prasanna, A. Gold-Parker, M.F. Toney, M.D. McGehee, Mechanism of Tin Oxidation and Stabilization by Lead Substitution in Tin Halide Perovskites, ACS Energy Letters. 2 (2017) 2159–2165. https://doi.org/10.1021/acsenergylett.7b00636.
[57] T. Leijtens, R. Prasanna, K.A. Bush, G.E. Eperon, J.A. Raiford, A. Gold-Parker, E.J. Wolf, S.A. Swifter, C.C. Boyd, H.-P. Wang, M.F. Toney, S.F. Bent, M.D. McGehee, Tin–lead halide perovskites with improved thermal and air stability for efficient all-perovskite tandem solar cells, Sustainable Energy Fuels. 2 (2018) 2450–2459. https://doi.org/10.1039/C8SE00314A.

[58] D. Meggiolaro, D. Ricciarelli, A.A. Alasmari, F.A.S. Alasmary, F. De Angelis, Tin versus Lead Redox Chemistry Modulates Charge Trapping and Self-Doping in Tin/Lead Iodide Perovskites, J. Phys. Chem. Lett. 11 (2020) 3546–3556. https://doi.org/10.1021/acs.jpclett.0c00725.
[59] D. Ricciarelli, D. Meggiolaro, F. Ambrosio, F. De Angelis, Instability of Tin Iodide Perovskites: Bulk p-Doping versus Surface Tin Oxidation, ACS Energy Lett. (2020) 2787–2795. https://doi.org/10.1021/acsenergylett.0c01174.
[60] L.E. Mundt, J. Tong, A.F. Palmstrom, S.P. Dunfield, K. Zhu, J.J. Berry, L.T. Schelhas, E.L. Ratcliff, Surface-Activated Corrosion in Tin–Lead Halide Perovskite Solar Cells, ACS Energy Lett. 5 (2020) 3344–3351. https://doi.org/10.1021/acsenergylett.0c01445.
[61] N. Aristidou, C. Eames, I. Sanchez-Molina, X. Bu, J. Kosco, M.S. Islam, S.A. Haque, Fast oxygen diffusion and iodide defects mediate oxygen-induced degradation of perovskite solar cells, Nat Commun. 8 (2017) 15218. https://doi.org/10.1038/ncomms15218.
[62] M.T. Klug, R.L. Milot, J.B. Patel, T. Green, H.C. Sansom, M.D. Farrar, A.J. Ramadan, S. Martani, Z. Wang, B. Wenger, J.M. Ball, L. Langshaw, A. Petrozza, M.B. Johnston, L.M. Herz, H.J. Snaith, Metal composition influences optoelectronic quality in mixed-metal lead–tin triiodide perovskite solar absorbers, Energy & Environmental Science. 13 (2020) 1776–1787. https://doi.org/10.1039/D0EE00132E.
[63] K.J. Savill, A.M. Ulatowski, L.M. Herz, Optoelectronic Properties of Tin–Lead Halide Perovskites, ACS Energy Lett. 6 (2021) 2413–2426. https://doi.org/10.1021/acsenergylett.1c00776.
[64] V.J.-Y. Lim, A.M. Ulatowski, C. Kamaraki, M.T. Klug, L. Miranda Perez, M.B. Johnston, L.M. Herz, Air-Degradation Mechanisms in Mixed Lead-Tin Halide Perovskites for Solar Cells, Advanced Energy Materials. n/a (n.d.) 2200847. https://doi.org/10.1002/aenm.202200847.
[65] E.S. Parrott, T. Green, R.L. Milot, M.B. Johnston, H.J. Snaith, L.M. Herz, Interplay of Structural and Optoelectronic Properties in Formamidinium Mixed Tin–Lead Triiodide Perovskites, Advanced Functional Materials. 28 (2018) 1802803. https://doi.org/10.1002/adfm.201802803.
[66] R.L. Milot, M.T. Klug, C.L. Davies, Z. Wang, H. Kraus, H.J. Snaith, M.B. Johnston, L.M. Herz, The Effects of Doping Density and Temperature on the Optoelectronic Properties of Formamidinium Tin Triiodide Thin Films, Advanced Materials. 30 (2018) 1804506. https://doi.org/10.1002/adma.201804506.
[67] L. Lanzetta, N. Aristidou, S.A. Haque, Stability of Lead and Tin Halide Perovskites: The Link between Defects and Degradation, J. Phys. Chem. Lett. 11 (2020) 574–585. https://doi.org/10.1021/acs.jpclett.9b02191.
[68] F. Wang, J. Ma, F. Xie, L. Li, J. Chen, J. Fan, N. Zhao, Organic Cation-Dependent Degradation Mechanism of Organotin Halide Perovskites, Advanced Functional Materials. 26 (2016) 3417–3423. https://doi.org/10.1002/adfm.201505127.
[69] M. Babics, M. De Bastiani, E. Ugur, L. Xu, H. Bristow, F. Toniolo, W. Raja, A.S. Subbiah, J. Liu, L.V. Torres Merino, E. Aydin, S. Sarwade, T.G. Allen, A. Razzaq, N. Wehbe, M.F. Salvador, S. De Wolf, One-year outdoor operation of monolithic perovskite/silicon tandem solar cells, Cell Reports Physical Science. 4 (2023) 101280. https://doi.org/10.1016/j.xcrp.2023.101280.
[70] R. Cheacharoen, C.C. Boyd, G.F. Burkhard, T. Leijtens, J.A. Raiford, K.A. Bush, S.F. Bent, M.D. McGehee, Encapsulating perovskite solar cells to withstand damp heat and thermal cycling, Sustainable Energy Fuels. 2 (2018) 2398–2406. https://doi.org/10.1039/C8SE00250A.
[71] Y. Tu, J. Wu, G. Xu, X. Yang, R. Cai, Q. Gong, R. Zhu, W. Huang, Perovskite Solar Cells for Space Applications: Progress and Challenges, Advanced Materials. 33 (2021) 2006545. https://doi.org/10.1002/adma.202006545.
[72] Excellent Intrinsic Long-Term Thermal Stability of Co-Evaporated MAPbI3 Solar Cells at 85 °C - Dewi - 2021 - Advanced Functional Materials - Wiley Online Library, (n.d.). https://onlinelibrary.wiley.com/doi/abs/10.1002/adfm.202100557 (accessed May 26, 2023).
[73] E. Aydin, T.G. Allen, M. De Bastiani, L. Xu, J. Ávila, M. Salvador, E. Van Kerschaver, S. De Wolf, Interplay between temperature and bandgap energies on the outdoor performance of

perovskite/silicon tandem solar cells, Nat Energy. 5 (2020) 851–859. https://doi.org/10.1038/s41560-020-00687-4.

[74] L.E. Mundt, F. Zhang, A.F. Palmstrom, J. Xu, R. Tirawat, L.L. Kelly, K.H. Stone, K. Zhu, J.J. Berry, M.F. Toney, L.T. Schelhas, Mixing Matters: Nanoscale Heterogeneity and Stability in Metal Halide Perovskite Solar Cells, ACS Energy Lett. 7 (2022) 471–480. https://doi.org/10.1021/acsenergylett.1c02338.

[75] T.A.S. Doherty, S. Nagane, D.J. Kubicki, Y.-K. Jung, D.N. Johnstone, A.N. Iqbal, D. Guo, K. Frohna, M. Danaie, E.M. Tennyson, S. Macpherson, A. Abfalterer, M. Anaya, Y.-H. Chiang, P. Crout, F.S. Ruggeri, S. Collins, C.P. Grey, A. Walsh, P.A. Midgley, S.D. Stranks, Stabilized tilted-octahedra halide perovskites inhibit local formation of performance-limiting phases, Science. 374 (2021) 1598–1605. https://doi.org/10.1126/science.abl4890.

[76] G.E. Eperon, T. Leijtens, K.A. Bush, R. Prasanna, T. Green, J.T.-W. Wang, D.P. McMeekin, G. Volonakis, R.L. Milot, R. May, A. Palmstrom, D.J. Slotcavage, R.A. Belisle, J.B. Patel, E.S. Parrott, R.J. Sutton, W. Ma, F. Moghadam, B. Conings, A. Babayigit, H.-G. Boyen, S. Bent, F. Giustino, L.M. Herz, M.B. Johnston, M.D. McGehee, H.J. Snaith, Perovskite-perovskite tandem photovoltaics with optimized band gaps, Science. 354 (2016) 861–865. https://doi.org/10.1126/science.aaf9717.